

# Northumbria Research Link

Citation: Wang, Zifang, Tian, Yakun, Wen, Ming, Wu, Qingsheng, Zhu, Qianjing and Fu, Yong Qing (2022) Integrating CoNiSe<sub>2</sub> Nanorod-arrays onto N-doped Sea-sponge-C spheres for highly efficient electrocatalysis of hydrogen evolution reaction. Chemical Engineering Journal, 446 (4). p. 137335. ISSN 1385-8947

Published by: Elsevier

URL: <https://doi.org/10.1016/j.cej.2022.137335>  
<<https://doi.org/10.1016/j.cej.2022.137335>>

This version was downloaded from Northumbria Research Link:  
<https://nrl.northumbria.ac.uk/id/eprint/49309/>

Northumbria University has developed Northumbria Research Link (NRL) to enable users to access the University's research output. Copyright © and moral rights for items on NRL are retained by the individual author(s) and/or other copyright owners. Single copies of full items can be reproduced, displayed or performed, and given to third parties in any format or medium for personal research or study, educational, or not-for-profit purposes without prior permission or charge, provided the authors, title and full bibliographic details are given, as well as a hyperlink and/or URL to the original metadata page. The content must not be changed in any way. Full items must not be sold commercially in any format or medium without formal permission of the copyright holder. The full policy is available online: <http://nrl.northumbria.ac.uk/policies.html>

This document may differ from the final, published version of the research and has been made available online in accordance with publisher policies. To read and/or cite from the published version of the research, please visit the publisher's website (a subscription may be required.)

# **Integrating CoNiSe<sub>2</sub> Nanorod-arrays onto N-doped Sea-sponge-C Spheres for highly efficient electrocatalysis of Hydrogen Evolution Reaction**

Zifang Wang<sup>a,‡</sup>, Yakun Tian<sup>a,‡</sup>, Ming Wen<sup>a,\*</sup>, Qingsheng Wu<sup>a</sup>, Qianjing Zhu<sup>a</sup>, Yong-Qing Fu<sup>b</sup>

<sup>a</sup> School of Chemical Science and Engineering, Shanghai Key Laboratory of Chemical Assessment and Sustainability, Tongji University, Shanghai 200092, China.

<sup>b</sup> Faculty of Engineering and Environment, Northumbria University, Newcastle upon Tyne NE99, UK.

\* Corresponding author Email: m\_wen@tongji.edu.cn.

‡ These authors contributed equally to this study.

**ABSTRACT.** A key issue for enhancing performance of hydrogen evolution reaction (HER) by utilizing seawater for sustainable clean energy is to develop a highly efficient, stable and economical electrocatalyst. Herein, a uniquely hierarchical nanostructure of CoNiSe<sub>2</sub> nanorod-arrays (NRAs) integrated onto N-doped sea-sponge-carbon spheres (CoNiSe<sub>2</sub>/N-SSCSs) was designed and synthesized using successive ultrasonic spray pyrolysis (USP) and solvothermal - hydrothermal selenization (SHS) processes. Attributed to intrinsic HER activity of CoNiSe<sub>2</sub> NRAs together with effective electron-transfer and ion-diffusion pathways of N-SSCSs, the CoNiSe<sub>2</sub>/N-SSCSs nanocomposites exhibited highly stable HER electrocatalytic performances in both alkaline electrolytes and alkaline simulated seawater. The required overpotential is as low as 88 mV with a Tafel slope of 83 mV dec<sup>-1</sup> at 10 mA cm<sup>-2</sup> in 1.0 M KOH, which are comparable to the electrode of commercial Pt/C ( $\eta_{10}$ = 35 mV &  $b$ =58 mV dec<sup>-1</sup>).

**Keywords:** CoNiSe<sub>2</sub> nanorod-arrays, Sea-sponge-C, hydrogen evolution reaction, electrocatalysis, seawater.

## 1. Introduction

Hydrogen energy is regarded as one of key green energy sources, and has merits of energy and environmental sustainability by using alkaline electrolyzers and abundant raw source [1-3]. However, it has been a key challenge to find an efficient and stable electrocatalyst to replace the expensive noble-metals (such as Pt) for hydrogen evolution reaction (HER) in an alkaline/neutral medium [4-10]. On another matter, seawater, as a rich water resource, has recently become a promising candidate for the electrolysis in hydrogen production [11-13]. Whereas its hard cations ( $\text{Ca}^{2+}$  and  $\text{Mg}^{2+}$ ) with negative potentials could be deposited on the surfaces of the catalysts in a form of hydroxides, thus blocking the active sites [14,15]. Besides, there is also a competing chlorine evolution reaction (CER) occurring at the counter electrode because of chloride electro-oxidation chemistry, which results in harmful chlorine or highly corrosive hypochlorite and destroys the structures of electrocatalysts [16-19]. Nevertheless, the above problems are believed to be effectively solved in an alkaline medium by using economical electrocatalysts with excellent stability and reliability during the electrolysis of seawater [20-22].

Transition-metal selenides (TMSs), with their outstanding cost effectiveness and relatively low intrinsic resistivity, have shown good electrochemical activities in a wide range of pH values for HER during the water splitting process [23-25]. Recently, ternary metal selenides have received extensive attention, because their synergistic effects of various elements can effectively adjust their electronic structures, thus enhancing the overall catalytic performance [26-29]. For example, in transition metal based ternary metal selenides (e.g.,  $\text{MWSe}_x$ : M= Co, Ni, Fe and Mn), the catalytic performance can be significantly enhanced by adding Ni or Co into  $\text{WSe}_x$  [30]. However, these TMSs have often shown poor electrical conductivities and unstable microstructures during water alkaline electrolysis [31-33]. Some porous carbonaceous materials were reported to accelerate

electron transfer and ion diffusion during the electrocatalytic reactions, including CNTs, carbon fibers (CFs) and porous carbon skeleton [34-36]. For example, N-doping porous carbon skeleton has been reported very effective due to its numerous active sites and increased electrical conductivity [37,38]. Therefore, we believe that hybrid and hierarchical nanostructures containing TMSs with a N-doped carbon skeleton may achieve enhanced electrical conductivity, rapid mass transfer, and large specific surface areas with abundant active sites, thus promising to realize good HER electrocatalytic performance [39].

In this work, CoNiSe<sub>2</sub> nanorod-arrays (NRAs) are uniformly grown on porous structured N-doped Sea-sponge-C spheres (N-SSCSs) [40,41] to form CoNiSe<sub>2</sub>/N-SSCSs nanocomposites through successive ultrasonic spray pyrolysis and solvothermal-hydrothermal selenization (USP-SHS) processes. Our unique design strategy is illustrated in Fig. 1. CoNi-precursor NRAs are uniformly grown onto N-SSCSs using a solvothermal process, and then hierarchically nanostructured CoNiSe<sub>2</sub>/N-SSCSs is successfully synthesized through the subsequent hydrothermal selenization process. When these active CoNiSe<sub>2</sub> NRAs are cross-linked with 3D conductive N-SSCSs, the number of active sites are increased significantly and effective pathways for electron-transfer and ion-diffusion are generated. Therefore, the hierarchically nanostructured CoNiSe<sub>2</sub>/N-SSCSs exhibits outstanding HER catalytic performance and stability in alkaline (1.0 M KOH), neutral (2.0 M PBS) media and also in alkaline simulated seawater. This work provides a unique strategy to develop high performance HER electrocatalysts with wide application prospects.

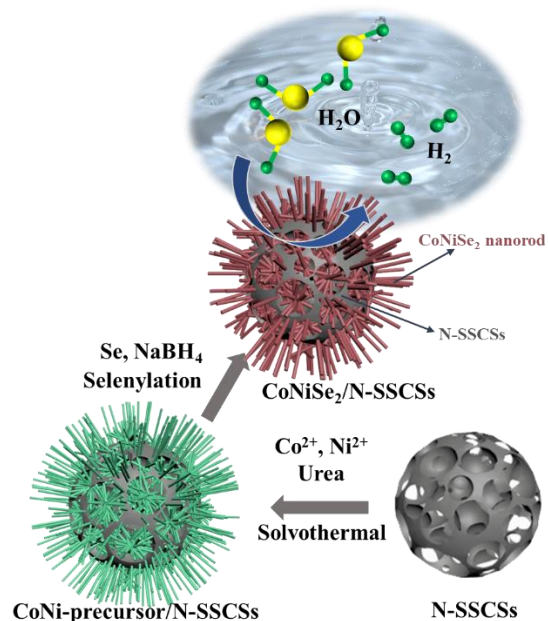


**Fig. 1.** Schematic illustrations for fabricating CoNiSe<sub>2</sub>/N-SSCSs nanocomposites.

## 2. Experimental

### 2.1 Synthesis of CoNiSe<sub>2</sub>/N-SSCSs electrocatalyst.

Nanocomposites of CoNiSe<sub>2</sub>/N-SSCSs were synthesized by integrating CoNi-precursor onto the N-SSCSs (Fig. S1) [40,41], followed by a selenization treatment. In a typical synthetic procedure, 0.2 mmol Ni(NO<sub>3</sub>)<sub>2</sub>·6H<sub>2</sub>O, 0.2 mmol Co(NO<sub>3</sub>)<sub>2</sub>·6H<sub>2</sub>O, 0.4 mmol urea and 2 mg N-SSCSs were added into a mixture of 16 mL deionized water and 4 mL ethanol. The mixture was ultrasonically mixed for 1 hour to ensure Co<sup>2+</sup> and Ni<sup>2+</sup> ions fully adsorbed onto the N-SSCSs. The mixed solution was then transferred to a 25 mL Teflon-lined stainless-steel autoclave, which was maintained at 120 °C for 4 hours and naturally cooled down to ambient temperature. The collected precursor was mixed with 20 mL NaHSe solution and then transferred into a 25 mL Teflon-lined stainless-steel autoclave under argon (Ar) gas. After the hydrothermal selenization treatment at 160 °C for 24 hours, the final product of CoNiSe<sub>2</sub>/N-SSCSs was collected by washing with deionized water and ethanol. It was then dried in a vacuum oven at 60 °C for 12 hours. The

synthesis parameters of control group samples such as CoNiSe<sub>2</sub>, NiSe<sub>2</sub>/N-SSCSs, CoSe<sub>2</sub>/N-SSCSs, NiSe<sub>2</sub> and CoSe<sub>2</sub> are described in the experimental section in the supporting information.

## 2.2 Characterization methods

Morphology and microstructures of the as-prepared samples were characterized using a field emission scanning electron microscope (FE-SEM, JEOL, S-4800), a transmission electron microscope (TEM), and a high-resolution TEM (HRTEM, JEOL JEM-2100EX microscopy). Crystalline structures of the samples were analyzed using a Bruker D8 advanced (German) diffractometer with a Cu K $\alpha$  radiation source ( $\lambda = 0.154056$  nm). Energy-dispersive X-ray spectroscopy (EDS, TN5400 EDS instrument, Oxford, operated at 15 keV) was used to obtain the elemental mapping of the samples. Chemical elements and their binding information were obtained using an X-ray photoelectron spectroscopy (XPS, Thermo Scientific K-Alpha spectrometer), with a monochromatized Al K $\alpha$  ( $h\nu = 1,486.6$  eV) X-ray source. The XPS peak of the contaminate carbon (C 1s = 284.6 eV) was used as the calibration reference of the binding energies.

## 2.3 Electrochemical measurements.

All the electrochemical tests were carried out using an electrochemical workstation (CHI 760E) with a standard three-electrode system, in which a saturated calomel electrode (SCE), a graphite rod and a 3 mm diameter glassy carbon electrode (GCE) loaded catalysts were used as the reference electrode, the counter electrode and the working electrode, respectively. The ink of electrocatalysts was prepared and 5  $\mu$ L of electrocatalysts slurry was dropped onto the polished GCE and dried at room temperature. Solutions of 1.0 M KOH, 2.0 M PBS, 0.5 M H<sub>2</sub>SO<sub>4</sub> and alkaline simulated seawater [42] were prepared as the electrolytes and saturated with Ar gas before testing. All the potentials measured in this work were referred to the reversible hydrogen electrode (RHE) using the equation of:  $E$  (RHE) =  $E$  (SCE) + 0.242 V + 0.0591  $\times$  pH. During measurements, 20 cycles

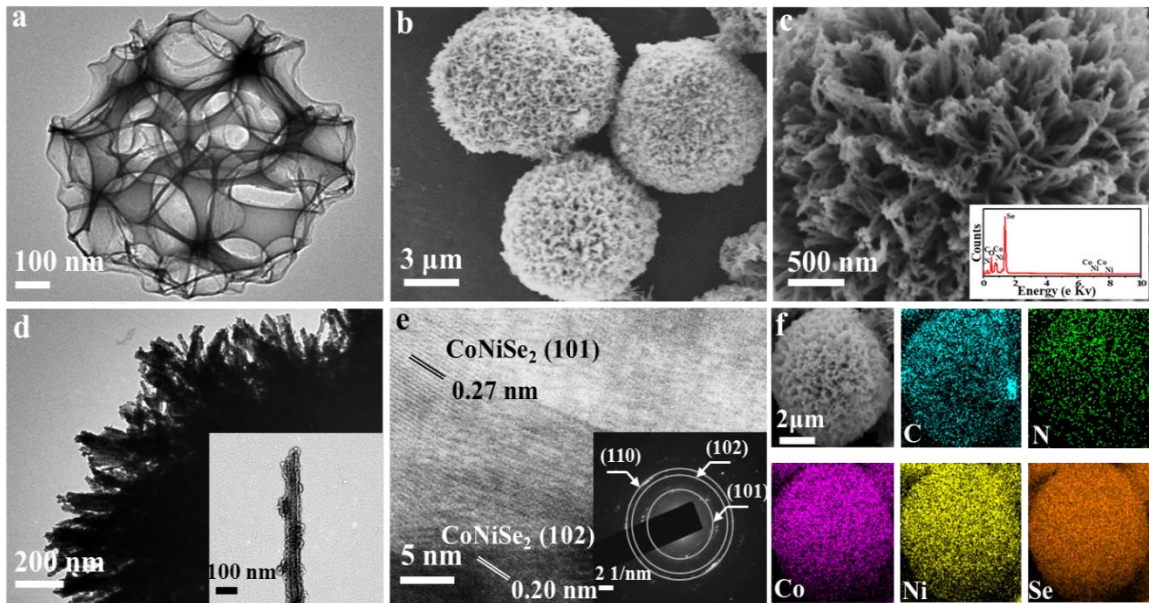
of cyclic voltammetry (CV) tests of the electrode materials in a potential window (0.2 ~ 0.6V vs. RHE.) without Faradaic currents were performed. Values of double layer capacitance ( $C_{dl}$ ) were derived by measuring the CV scans at different scanning rates of 20, 40, 60, 80 and 100  $\text{mV s}^{-1}$ . Linear sweep voltammetry (LSV) was conducted at a scan rate of 2  $\text{mV s}^{-1}$  to compare the electrochemical activities of the as-prepared samples. Manual  $iR$  correction was carried out for all the polarization curves according to the equation of:  $E_{\text{compensated}} = E_{\text{measured}} - i \times R_s$ , in which  $R_s$  is the series resistance measured by electrochemical impedance spectroscopy (EIS). Tafel plots were obtained based on the results of overpotential ( $\eta$ ) versus log current ( $\log j$ ) in polarization curves to evaluate the HER kinetics of catalysts. The Tafel equation is obtained using the equation of  $\eta = b \log(j) + a$ , where  $b$  (Tafel slope) represents the intrinsic activity of the catalysts and is used to analyze the rate-determining step of the HER process. EIS measurements were obtained within the frequency range of  $10^5$  to 0.01 Hz, with an AC voltage amplitude of 5 mV. In addition, chronoamperometry tests were conducted to evaluate the electrochemical HER stability of catalysts which were tested for 12 hours.

### 3. Results and discussion

#### 3.1 Synthesis and Characterization

Fig. 2 presents the morphology and structure of  $\text{CoNiSe}_2/\text{N-SSCSs}$  obtained by the USP-SHS processes. In the fabrication, urea was selected to decompose  $\text{CO}_3^{2-}$  and  $\text{OH}^-$  for co-precipitating  $\text{Ni}^{2+}$  and  $\text{Co}^{2+}$  adsorbed onto N-SSCSs in the solvothermal system, and CoNi-precursor of NRAs were generated on N-SSCSs due to its lower nucleation barrier (Fig. S2). The phase transformation during the hydrothermal selenization process produced the  $\text{CoNiSe}_2$  NRAs/N-SSCSs (Fig. S3). However, there are many quite messy nanorods of  $\text{CoNiSe}_2$  without N-SSCSs (Fig. S4). The reaction conditions were further optimized (Figs. S5-S6). From the TEM image shown in Fig. 2a,

the amorphous N-SSCSs has a 3D interpenetrating and porous structure with the aperture size of 300-500 nm. SEM and TEM images show that CoNiSe<sub>2</sub> NRAs are inserted uniformly into N-SSCSs skeleton (Figs. 2b-d). Fig. 2e shows a HRTEM image of a single CoNiSe<sub>2</sub> nanorod (the inset of Fig. 2d). It clearly shows lattice fringes of 0.27 and 0.20 nm, which correspond to the (101) and (102) planes of CoNiSe<sub>2</sub>, respectively. The corresponding selected-area electron diffraction (SAED) pattern (the inset of Fig. 2e) reveals the polycrystalline nature of CoNiSe<sub>2</sub>/N-SSCSs. EDS spectrum (the inset of Fig. 2c) and elemental mapping (Fig. 2f) confirm the uniform distribution of C, N, Co, Ni, and Se, which demonstrates the existence of N-SSCSs by comparing the EDS results of CoNiSe<sub>2</sub> NRAs.



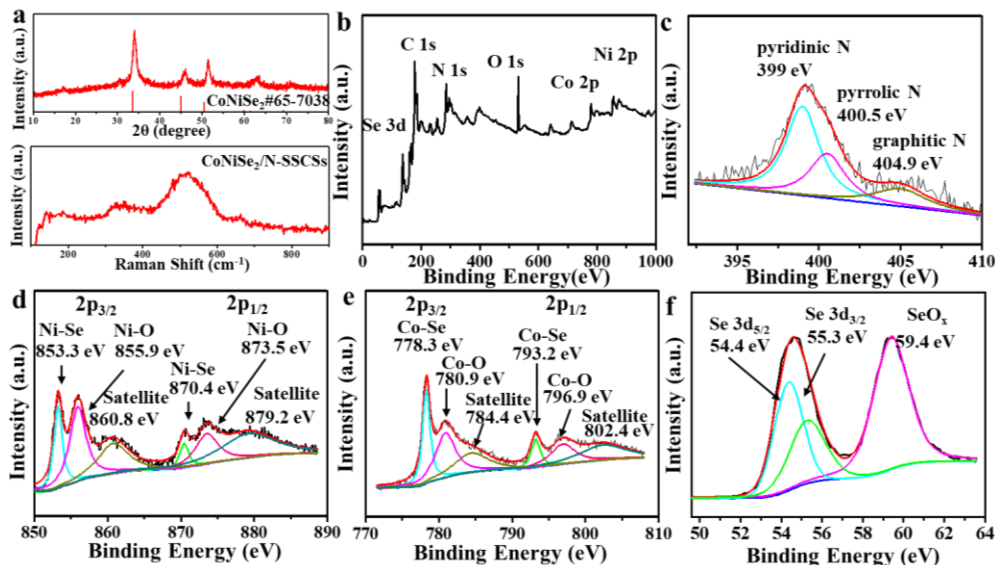
**Fig. 2.** Material characterization: (a) TEM image of N-SSCSs. (b, c) SEM images in different magnifications (Inset: EDS), (d) TEM images (Inset: a single nanorod of CoNiSe<sub>2</sub>), (e) HRTEM image (Inset: SAED pattern), (f) Elemental mapping of CoNiSe<sub>2</sub>/N-SSCSs.

Fig. 3 shows the crystalline phases and elemental valance states of the prepared samples. XRD pattern shows that the CoNiSe<sub>2</sub>/N-SSCSs presents three major peaks at  $2\theta$  values of 32.9°, 44.4° and 49.9°, corresponding to the (101), (102) and (110) planes of CoNiSe<sub>2</sub> (PDF# 65-7038). Whereas that of the N-SSCSs only shows a broad diffraction peak of amorphous structure (Fig. 3a,

above). Raman spectrum (Fig. 3a, below) of CoNiSe<sub>2</sub>/N-SSCSs exhibits band near 520 cm<sup>-1</sup> ascribed to A<sub>g</sub> symmetric stretching mode. The band located near 208 cm<sup>-1</sup> is attributed to the stretching vibration mode of the Se-Se pair. The bands observed near 477 and 680 cm<sup>-1</sup> are the Raman vibration modes of CoNiSe<sub>2</sub>/N-SSCSs [43,44]. Raman spectra of SSCSs and N-SSCSs reveal that the value of I<sub>D</sub>:I<sub>G</sub> is increased from 0.72 to 0.83 after N-doping, indicating that the N-doping increases the defect degree of SSCSs.

XPS analysis was performed to investigate the valence states and elemental binding information. In Fig. 3b, the XPS survey spectrum reveals peaks of Se 3d, C 1s, N 1s, O 1s, Ni 2p, and Co 2p in the binding energy region from 0 to 1000 eV, which are consistent with the EDS results. The C 1s spectrum (Fig. S7) can be deconvoluted into three peaks centered at 284.3, 285.4 and 287.8 eV, corresponding to C-C/C=C, C-O/C-N and C=O/C=N, respectively [45,46]. The existence of N-C (sp<sup>2</sup>)- and N-C (sp<sup>3</sup>)- type bonds indicates that nitrogen is successfully integrated into the N-SSCSs structure. High-resolution N 1s spectrum (Fig. 3c) can be deconvoluted into three peaks, namely pyridinic N at 399 eV, pyrrolic N at 400.5 eV and graphitic N at 404.9 eV, respectively [47,48]. The presence of pyridine N and pyrrole N is beneficial for the electrocatalytic activity of HER process through actively interacting with H<sup>+</sup> [39]. High-resolution spectrum of Ni 2p can be deconvoluted into three pairs of peaks (Fig. 3d). The two peaks at 860.8 and 879.2 eV are ascribed to the satellite peaks of Ni 2p [49]. The two main peaks located at 853.3 and 870.4 eV correspond to Ni 2p<sub>3/2</sub> and Ni 2p<sub>1/2</sub>, respectively, which can be assigned to Ni-Se bonds [50,51]. The other two peaks at 855.9 and 873.5 eV are attributed to partially oxidized bonds as a result of the sample's exposure to air [52]. For the high resolution spectrum of Co 2p (Fig. 3e), two spin-orbit peaks are at 778.3 and 793.2 eV, referring to Co 2p<sub>3/2</sub> and Co 2p<sub>1/2</sub>, together with two satellite peaks at 784.4 and 802.4 eV [53], representing Co-Se bonds [54]. The peaks at 780.9 and 796.9 eV can be

attributed to Co-O bonds [53]. In Fig. 3f, the high resolution spectrum of Se 3d is resolved into two main peaks at 54.4 and 55.3 eV, corresponding to Se 3d<sub>5/2</sub> and Se 3d<sub>3/2</sub>, which are related to the metal-selenium interactions. Meanwhile, the signal at 59.4 eV is linked to the existence of SeO<sub>x</sub>, due to the oxidation in air. [55]. In brief, XPS results confirm the formation of CoNiSe<sub>2</sub> NRAs on the N-SSCSs.



**Fig. 3.** (a) XRD pattern (above) and Raman spectrum (below) of CoNiSe<sub>2</sub>/N-SSCSs; (b) XPS full spectrum of CoNiSe<sub>2</sub>/N-SSCSs; (c-f) High resolution XPS spectra of N 1s, Ni 2p, Co 2p, Se 3d, respectively.

### 3.2 Electrocatalytic HER performance.

To evaluate its electrocatalytic performance for HER, the as-synthesized CoNiSe<sub>2</sub>/N-SSCSs was tested in a 1.0 M KOH solution using a typical three-electrode system. The obtained results are shown in Fig. 4. The polarization curves after *iR*-drop corrections and Tafel slopes are illustrated in Figs. 4a-c. The CoNiSe<sub>2</sub>/N-SSCSs shows a superior activity with a low overpotential of 88 mV and a Tafel slope of 83 mV dec<sup>-1</sup> at 10 mA cm<sup>-2</sup>. These readings are dramatically different from those of the single-metal counterparts of NiSe<sub>2</sub>/N-SSCSs ( $\eta_{10}$ =135 mV &  $b$ =102 mV dec<sup>-1</sup>, Fig. S8) and CoSe<sub>2</sub>/N-SSCSs ( $\eta_{10}$ =162 mV &  $b$ =104 mV dec<sup>-1</sup>, Fig. S9). These values are comparable to those of the commercial Pt/C ( $\eta_{10}$ = 35 mV &  $b$ =58 mV dec<sup>-1</sup>) and are also very

prominent compared with those of Se-based and CoNiSe<sub>2</sub>-based HER catalysts reported in literature (Table S1-S2). However, the N-SSCSs have both a large overpotential and a large Tafel slope due to inert HER catalysis. In particular, the overpotentials and Tafel slopes of CoNiSe<sub>2</sub>/N-SSCSs, NiSe<sub>2</sub>/N-SSCSs and CoSe<sub>2</sub>/N-SSCSs are all better than those of CoNiSe<sub>2</sub>, NiSe<sub>2</sub> and CoSe<sub>2</sub>. These results indicate the acceleration of N-SSCSs for HER reaction kinetics based on 3D crosslinking channels and good conductivity, thus improving the HER performance. The CoNiSe<sub>2</sub> ( $\eta_{10}=158$  mV &  $b=101$  mV dec<sup>-1</sup>) shows a much better performance than NiSe<sub>2</sub> ( $\eta_{10}=179$  mV &  $b=117$  mV dec<sup>-1</sup>, Fig. S10) and CoSe<sub>2</sub> ( $\eta_{10}=179$  mV &  $b=115$  mV dec<sup>-1</sup>, Fig. S11). Therefore, we can conclude that alloying with Co and Ni atoms is an effective method to enhance the performance of CoNiSe<sub>2</sub>/N-SSCSs. The optimized Co:Ni ratio of 1:1 in the CoNiSe<sub>2</sub>/N-SSCSs exhibits the lowest overpotential than those with other Co:Ni ratios (Fig. S12). Theoretically, when the reactions follow the Volmer, Heyrovsky and Tafel mechanisms, the Tafel slopes are 119 mV dec<sup>-1</sup>, 40 mV dec<sup>-1</sup> and 30 mV dec<sup>-1</sup>, respectively [56]. The lowest Tafel slope of CoNiSe<sub>2</sub>/N-SSCSs at 83 mV dec<sup>-1</sup> located within 119~40 mV dec<sup>-1</sup> indicates that it has the fast reaction kinetics via the Volmer-Heyrovsky reaction mechanism [57].

EIS measurements were performed under a potential of 180 mV for the prepared samples. The obtained results are plotted in Fig. 4d. The obtained charge transport impedance ( $R_{ct}$ ) of CoNiSe<sub>2</sub>/N-SSCSs is 48  $\Omega$ , which is lower than those of NiSe<sub>2</sub>/N-SSCSs (60.5  $\Omega$ ), CoSe<sub>2</sub>/N-SSCSs (84.7  $\Omega$ ), CoNiSe<sub>2</sub> (67  $\Omega$ ), NiSe<sub>2</sub> (69.3  $\Omega$ ) and CoSe<sub>2</sub> (90.9  $\Omega$ ). This suggests that the synergistic effect between Co and Ni atoms as well as the porous structure of conductive N-SSCSs improve the conductivity and charge transfer rate. For the CoNiSe<sub>2</sub>/N-SSCSs applied with varied overpotentials, the  $R_{ct}$  value decreases gradually with the increase of overpotential, indicating that charge transfer kinetics is accelerated with the increase of overpotential (Fig. S13) [58]. To further

investigate the intrinsic activities of the electrocatalysts, the  $C_{dl}$  was obtained by testing the CVs at different sweep speeds in the non-redox potential region (Fig. S14). Fig. 4e shows that the  $C_{dl}$  value of CoNiSe<sub>2</sub>/N-SSCSs is much higher than those of NiSe<sub>2</sub>/N-SSCSs, CoSe<sub>2</sub>/N-SSCSs, CoNiSe<sub>2</sub>, NiSe<sub>2</sub> and CoSe<sub>2</sub>. This is mainly because there are more catalytically active sites in CoNiSe<sub>2</sub>/N-SSCSs, which are all available for the HER. The long-term stability was further investigated for the prepared samples using the chronoamperometry, and the obtained results are shown in Fig. 4f. Compared with that of CoNiSe<sub>2</sub> (Fig. S15), the CoNiSe<sub>2</sub>/N-SSCSs exhibits the highest and stable current density at an overpotential of 200 mV without apparent decays within 12 hours. There are no obvious morphology changes of CoNiSe<sub>2</sub>/N-SSCSs after the durability test (Fig. S16), showing no apparent aggregation or morphology changes of CoNiSe<sub>2</sub> NRAs. The Faraday efficiency (FE) of CoNiSe<sub>2</sub>/N-SSCSs in the 1.0 M KOH solution was evaluated by using a sealed H-type electrolytic cell with a proton membrane to quantitatively collect the H<sub>2</sub>. The result is compared with the theoretical value of H<sub>2</sub> calculated using the Faraday Law (Fig. S17). Fig. 4g shows that the measured H<sub>2</sub> amount (the inset of Fig. 4g) keeps increasing continuously. The amount of H<sub>2</sub> collected within 15 minutes is 0.21 mmol, corresponding to a high FE value of 94% [59,60]. In addition, the turnover frequency (TOF) value of CoNiSe<sub>2</sub>/N-SSCSs is calculated to be 0.28 s<sup>-1</sup> at an overpotential of 130 mV at pH = 7 (Fig. S18), which indicates CoNiSe<sub>2</sub>/N-SSCSs has the high intrinsic HER activity [61]. The HER mechanism of CoNiSe<sub>2</sub>/N-SSCSs in the alkaline medium is illustrated in Fig. 4h. The alloying of Co and Ni atoms improves the intrinsic conductivity and specific surface areas of the electrocatalyst. This regulates Gibbs free energy ( $\Delta G$ ) for adsorption of hydrogen intermediates (H<sub>ads</sub>) and the free energy of water dissociation to form H<sub>ads</sub> and OH<sup>-</sup> in the Volmer step [62,63]. The Volmer step thus has also been enhanced by the CoNiSe<sub>2</sub>/N-SSCSs catalyst. Moreover, the presence of N-SSCSs enables the CoNiSe<sub>2</sub> NRAs to

expose numerous catalytic active sites, which affords efficient electron transfer channels as shown in Fig. 4h.

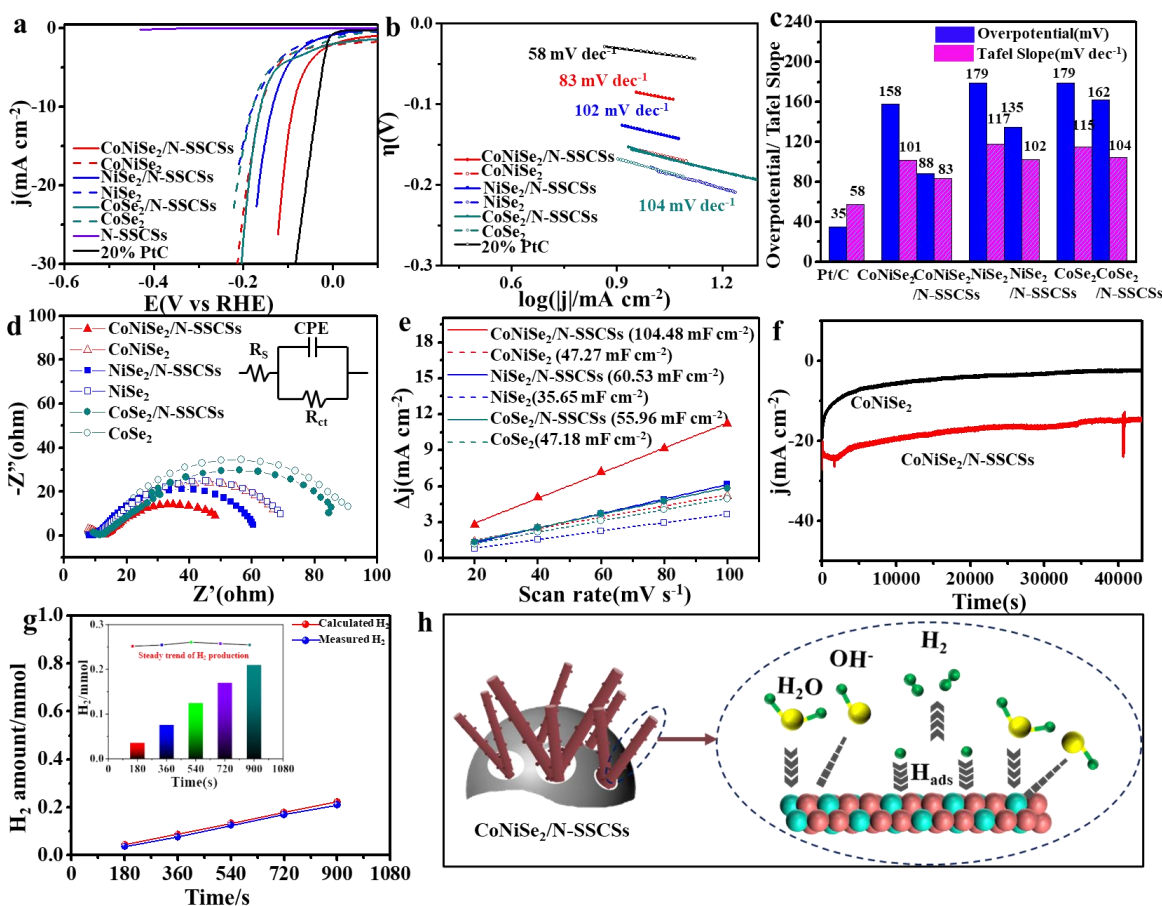


**Fig. 4.** HER performances of the as-prepared samples in 1.0 M KOH: (a) Polarization curves; (b) Tafel plots; (c) Values of the overpotential and Tafel slope at 10 mA cm<sup>-2</sup>, (d) Nyquist plots (Inset: the equivalent circuit modeling to fit all the EIS data); (e) C<sub>dl</sub> values; (f) Chronoamperometry curves of the prepared samples; (g) The amount of H<sub>2</sub> theoretically calculated and experimentally measured versus time (Inset: gas collection of H<sub>2</sub>); (h) Schematic illustration of the HER activity of CoNiSe<sub>2</sub>/N-SSCSs in the alkaline medium.

The HER performance of the as-prepared electrocatalysts was further evaluated in a 2.0 M PBS solution (with a pH value of 7) to evaluate their practical applications. The obtained results are shown in Fig. 5, and they are similar to those obtained in a 1.0 M KOH. As shown in Figs. 5a-c, the CoNiSe<sub>2</sub>/N-SSCSs shows an overpotential of 162 mV and a Tafel slope of 116 mV dec<sup>-1</sup> at 10 mA cm<sup>-2</sup>. These values are comparable to those of the commercial Pt/C ( $\eta_{10}$ =85 mV,  $b$ =187 mV dec<sup>-1</sup>).

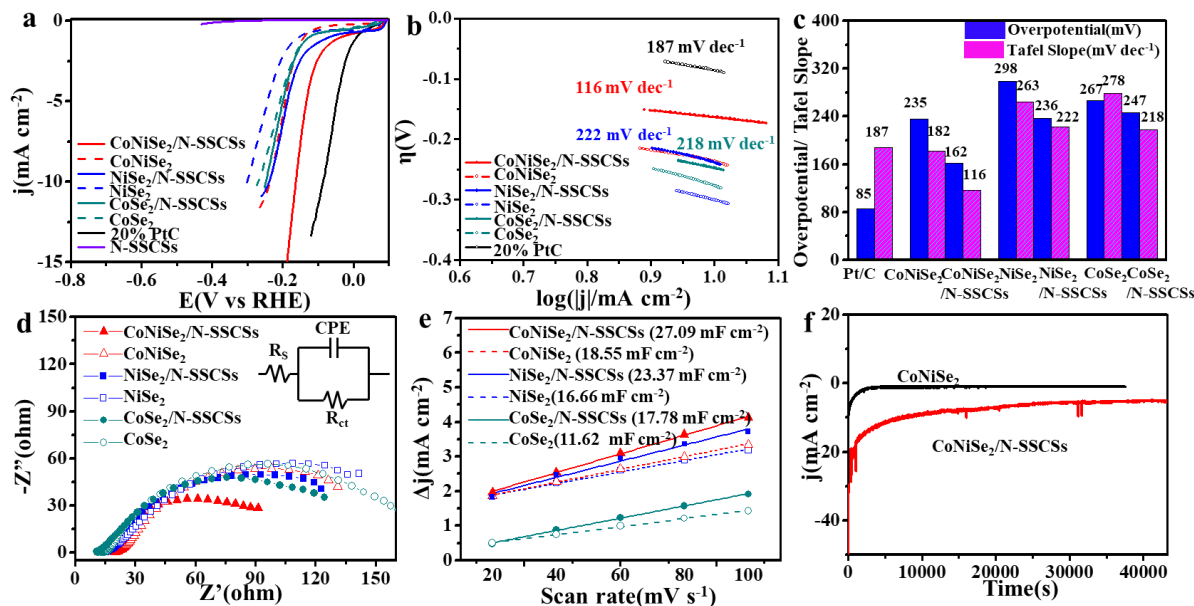


**Fig. 5.** HER performances of the as-prepared samples in 2.0 M PBS: (a) Polarization curves; (b) Tafel plots; (c) Values of the overpotential and Tafel slope at  $10 \text{ mA cm}^{-2}$ , (d) Nyquist plots (Inset: the equivalent circuit modeling to fit all the EIS data); (e)  $C_{dl}$  values; (f) Chronoamperometry curves of the prepared samples.

Based on the Volmer-Heyrovsky reaction mechanism [57],  $\text{CoNiSe}_2/\text{N-SSCSs}$  has a superior HER performance in 2.0 M PBS, compared to the control group samples, including  $\text{NiSe}_2/\text{N-SSCSs}$  ( $\eta_{10}=236 \text{ mV}$ ,  $b=222 \text{ mV dec}^{-1}$ ),  $\text{CoSe}_2/\text{N-SSCSs}$  ( $\eta_{10}=247 \text{ mV}$ ,  $b=218 \text{ mV dec}^{-1}$ ),  $\text{CoNiSe}_2$  ( $\eta_{10}=235 \text{ mV}$ ,  $b=182 \text{ mV dec}^{-1}$ ),  $\text{NiSe}_2$  ( $\eta_{10}=298 \text{ mV}$ ,  $b=263 \text{ mV dec}^{-1}$ ) and  $\text{CoSe}_2$  ( $\eta_{10}=267 \text{ mV}$ ,  $b=278 \text{ mV dec}^{-1}$ ), mainly due to rate-limiting steps of Volmer reactions for those control group samples [57]. Furthermore, the  $\text{CoNiSe}_2/\text{N-SSCSs}$  shows a much lower  $R_{ct}$  value of  $91 \Omega$  (At the overpotential of 220 mV) and a higher  $C_{dl}$  value of  $27.09 \text{ mF cm}^{-2}$  than those of  $\text{NiSe}_2/\text{N-SSCSs}$ ,  $\text{CoSe}_2/\text{N-SSCSs}$ ,  $\text{CoNiSe}_2$ ,  $\text{NiSe}_2$  and  $\text{CoSe}_2$  (Figs. 5d-e, Fig. S19). Comparing the stability of  $\text{CoNiSe}_2/\text{N-SSCSs}$  and  $\text{CoNiSe}_2$  at 300mV,  $\text{CoNiSe}_2/\text{N-SSCSs}$  can remained a stable current density within 12 hours, while the current density  $\text{CoNiSe}_2$  decreases more seriously (Fig. 5f, Fig. S20). There are no obvious morphological changes in the both samples. All the above results show that the  $\text{CoNiSe}_2/\text{N-SSCSs}$  has both excellent electrocatalytic activity and stability for HER in alkaline/neutral electrolytes.

### 3.3 Electrocatalytic HER performance in alkaline simulated seawater.

To demonstrate the practical applications, the prepared electrocatalysts were tested in the alkaline simulated seawater, and the obtained results are shown in Fig. 6. In Figs. 6a-c, CoNiSe<sub>2</sub>/N-SSCSs shows the best electrocatalytic activity in the alkaline simulated seawater, with an overpotential of 105 mV at 10 mA cm<sup>-2</sup>. This value is much better than those of control group samples (e.g., NiSe<sub>2</sub>/N-SSCSs (145 mV), CoSe<sub>2</sub>/N-SSCSs (175 mV), CoNiSe<sub>2</sub> (150 mV), NiSe<sub>2</sub> (169 mV) and CoSe<sub>2</sub> (187 mV)) and is closer to that of the commercial Pt/C (26 mV). Its smallest Tafel slope of 78 mV dec<sup>-1</sup> among all the catalysts in this study suggests its fastest kinetics via a Volmer-Heyrovsky mechanism toward the HER, compared with all the control group samples [57].

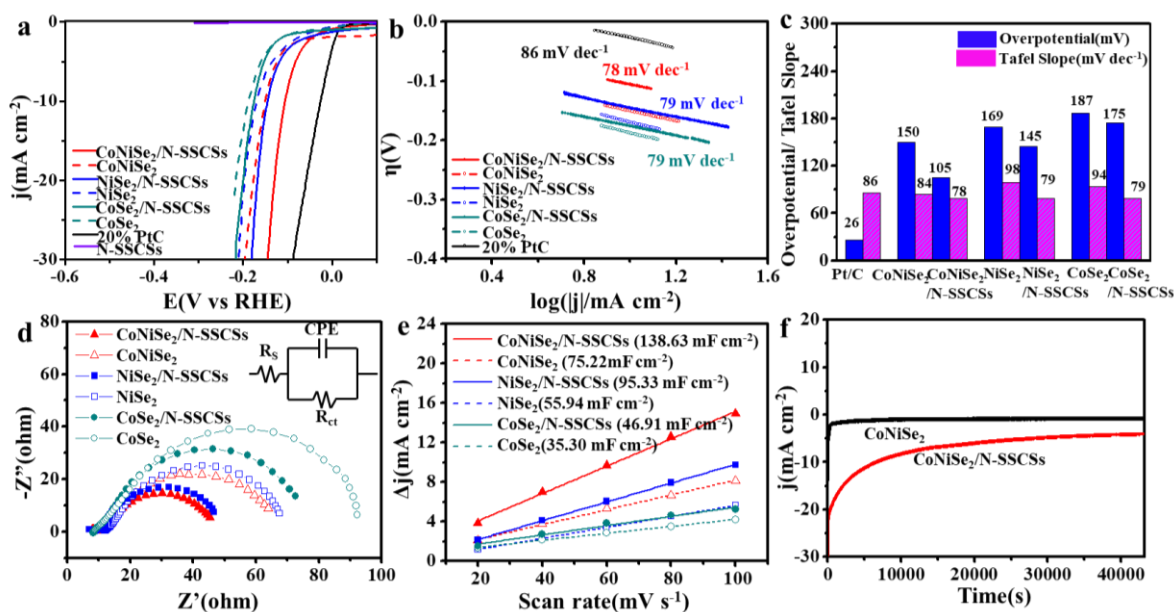


**Fig. 6.** HER performances of the as-prepared samples in alkaline simulated seawater : (a) Polarization curves; (b) Tafel plots; (c) Values of the overpotential and Tafel slope at 10 mA cm<sup>-2</sup>, (d) Nyquist plots (Inset: the equivalent circuit modeling to fit all the EIS data); (e)  $C_{dl}$  values; (f) Chronoamperometry curves of the prepared samples.

Meanwhile, studies using the EIS were done under the same overpotential of 180 mV for as-prepared samples mentioned above. CoNiSe<sub>2</sub>/N-SSCSs has the smallest  $R_{ct}$  value (Fig. 6d), consisting with its higher conductivity and faster charge transfer. Its largest  $C_{dl}$  value of 138.63

mF cm<sup>-2</sup> (Fig. 6e and Fig. S21) indicates that CoNiSe<sub>2</sub> NRAs are evenly distributed inside the N-SSCSs skeleton, which significantly increases the electrochemical active areas. In addition, the stability of CoNiSe<sub>2</sub>/N-SSCSs is superior to that of CoNiSe<sub>2</sub> at the potential of 200 mV, and it can maintain good performance within 12 hours without obvious degradation (Fig. 6f) and morphological changes.

#### **4. Conclusions**

In conclusion, a hierarchically nanostructured CoNiSe<sub>2</sub>/N-SSCSs was designed, synthesized and applied as electrocatalyst for HER. Owing to the uniformly growth of CoNiSe<sub>2</sub> NRAs onto the conductive porous N-SSCSs, the number of exposed active sites are significantly increased, and both the electron transfer and ion diffusion are accelerated simultaneously. Meanwhile, the synergistic effect between Co and Ni atoms effectively modulates the  $\Delta G$  of H<sub>ads</sub> adsorption and the free energy of water dissociation in Volmer step. The synthesized CoNiSe<sub>2</sub>/N-SSCSs electrocatalyst exhibits the superior electrocatalytic performance and long-term durability for HER in alkaline electrolyte and alkaline simulated seawater. This work provides a new idea for electrocatalytic HER in both alkaline electrolytes and seawater.

## **CRedit authorship contribution statement**

**Zifang Wang:** Writing-original draft, Investigation. **Yakun Tian:** Writing-original draft, Investigation. **Ming Wen:** Conceptualization, Writing-review & editing. **Qingsheng Wu:** Writing-review & editing. **Quanjing Zhu:** Writing-review & editing. **Yongqing Fu:** Investigation, Writing-review & editing.

## **Declaration of Competing Interest**

The authors declare that they have no known competing financial interests or personal relationships that could have appeared to influence the work reported in this paper.

## **Acknowledgements**

This work was financially supported by the National Natural Science Foundation (NSFC Nos: 22171212), Science and Technology Committee of Shanghai Municipality (21160710300, 19DZ2271500) by China, International Exchange Grant (IEC/NSFC/201078) through Royal Society UK and NSFC.

## **Appendix A. Supplementary data**

Supplementary data to this article can be found online at

## References

- [1] Y.T. Luo, L. Tang, U. Khan, Q.M. Yu, H.M. Cheng, X.L. Zou, B.L. Liu, Morphology and surface chemistry engineering toward pH-universal catalysts for hydrogen evolution at high current density, *Nat. Commun.* 10 (2019) 269.
- [2] Z.W. She, J. Kibsgaard, C.F. Dickens, I. Chorkendorff, J.K. Nørskov, T.F. Jaramillo, Combining theory and experiment in electrocatalysis: Insights into materials design, *Science* 355 (2017) 146.
- [3] C.Q. Li, J.B. Beak, The promise of hydrogen production from alkaline anion exchange membrane electrolyzers, *Nano Energy* 87(2021) 106162.
- [4] Y.K. Zhang, G. Yan, Y. Shi, H.Q. Tan, Y.G. Li, A branch-leaf-like hierarchical self-supporting electrode as a highly efficient catalyst for hydrogen evolution, *New J. Chem.* 45(2021) 10890.
- [5] Y.K. Tian, A.J. Huang, Z.G. Wang, M.K. Wang, Q.S. Wu, Y. Shen, Q.J. Zhu, Y.Q. Fu, M. Wen, Two-dimensional hetero-nanostructured electrocatalyst of Ni/NiFe-layered double oxide for highly efficient hydrogen evolution reaction in alkaline medium, *Chem. Eng. J.* 426 (2021) 131827.
- [6] B. Geng, F. Yan, X. Zhang, Y.Q. He, C.L. Zhu, S.L. Chou, X.L. Zhang, Y.J. Chen, Conductive CuCo-Based Bimetal Organic Framework for Efficient Hydrogen Evolution, *Adv. Mater.* 33 (2021) 2106781.
- [7] J. Kim, H.J. Jung, S.M. Jung, J.W. Hwang, D.Y. Kim, N.H. Lee, K.S. Kim, H. Kwon, Y.T. Kim, J.W. Han, J.K. Kim, Tailoring Binding Abilities by Incorporating Oxophilic Transition Metals on 3D Nanostructured Ni Arrays for Accelerated Alkaline Hydrogen Evolution Reaction, *J. Am. Chem. Soc.* 143 (2021) 1399-1408.
- [8] G.T. Zan, T. Wu, Z.L. Zhang, J. Li, J.C. Zhou, F. Zhu, H.X. Chen, M. Wen, X.C. Yang, X.J.

- Peng, J. Chen, Q.S. Wu, Bioinspired Nanocomposites with Self-adaptive Stress Dispersion for Super-Foldable Electrodes. *Adv. Sci.*, 9 (2022) 2103714.
- [9] G.F. Qian, J.L. Chen, T.Q. Yu, J.C. Liu, L. Luo, S.B. Yin, Three-Phase Heterojunction NiMo-Based Nano-Needle for Water Splitting at Industrial Alkaline Condition, *Nano-Micro Lett.* 14 (2022) 20.
- [10] L. Yan, B. Zhang, J.L. Zhu, Y.Y. Li, P. Tsiakaras, P.K. Shen, Electronic modulation of cobalt phosphide nanosheet arrays via copper doping for highly efficient neutral-pH overall water splitting, *Appl. Catal. B: Environ.* 265 (2020) 118555.
- [11] R. d'Amore-Domenech, O. Santiago, T.J. Leo, Multicriteria analysis of seawater electrolysis technologies for green hydrogen production at sea, *Renew. Sust. Energ. Rev.* 133 (2020), 110166.
- [12] Y. Kuang, M.J. Kenney, Y.T. Meng, W.H. Hung, Y.J. Liu, J.E. Huang, R. Prasanna, P.S. Li, Y.P. Li, L. Wang, M.C. Lin, M.D. McGehee, X.M. Sun, H.J. Dai, Solar-driven, highly sustained splitting of seawater into hydrogen and oxygen fuels, *Proc. Natl. Acad. Sci. U.S.A.* 116 (2019) 6624-6629.
- [13] S. Dresp, F. Dionigi, M. Klingenhof, P. Strasser, Direct Electrolytic Splitting of Seawater: Opportunities and Challenges, *ACS Energy Lett.* 4 (2019) 933-942.
- [14] L. Yu, L.B. Wu, B. McElhenny, S.W. Song, D. Luo, F.H. Zhang, Y. Yu, S. Chen, Z.F. Ren, Ultrafast room-temperature synthesis of porous S-doped Ni/Fe (oxy)hydroxide electrodes for oxygen evolution catalysis in seawater splitting, *Energy Environ. Sci.* 13 (2020) 3439.
- [15] Y.C. Huang, L. Hu, R. Liu, Y.W. Hu, T.Z. Xiong, W.T. Qiu, M. (J. Tang) Baloguna, A.L. Pan, Y.X. Tong, Nitrogen treatment generates tunable nanohybridization of Ni<sub>5</sub>P<sub>4</sub> nanosheets with nickel hydr(oxy)oxides for efficient hydrogen production in alkaline, seawater and acidic

- media, *Appl. Catal. B: Environ.* 251 (2019) 181-194.
- [16] Y.C. Li, X.Y. Wu, J.P. Wang, H.X. Wei, S.Y. Zhang, S.L. Zhu, Z.Y. L, S.L. Wu, H. Jiang, Y. Q. Liang, Sandwich structured Ni<sub>3</sub>S<sub>2</sub>-MoS<sub>2</sub>-Ni<sub>3</sub>S<sub>2</sub>@Ni foam electrode as a stable bifunctional electrocatalyst for highly sustained overall seawater splitting, *Electrochim. Acta* 390(2021) 138833.
- [17] Z.P. Yu, J.Y. Xu, L.J. Meng, L.F. Liu, Efficient hydrogen production by saline water electrolysis at high current densities without the interfering chlorine evolution, *J. Mater. Chem. A* 9 (2021) 22248.
- [18] S. Dresp, T.N. Thanh, M. Klingenhof, S. Bruckner, P. Hauke, P. Strasser, Efficient direct seawater electrolyzers using selective alkaline NiFe-LDH as OER catalyst in asymmetric electrolyte feeds, *Energy Environ. Sci.* 13 (2020) 1725.
- [19] W.M. Tong, M. Forster, F. Dionigi, S. Dresp, R. S. Erami, P. Strasser, A. J. Cowan, P. Farràs, Electrolysis of low-grade and saline surface water, *Nat. Energy* 5(2020) 367-377.
- [20] H.Y. Jin, X.S. Wang, C. Tang, A. Vasileff, L.Q. Li, A. Slattery, S.Z. Qiao, Stable and Highly Efficient Hydrogen Evolution from Seawater Enabled by an Unsaturated Nickel Surface Nitride, *Adv. Mater.* 33 (2021) 2007508.
- [21] K. Jiang, W.J. Liu, W. Lai, M.L. Wang, Q. Li, Z.L. Wang, J.J. Yuan, Y.L. Deng, J. Bao, H.B. Ji, NiFe Layered Double Hydroxide/FeOOH Heterostructure Nanosheets as an Efficient and Durable Bifunctional Electrocatalyst for Overall Seawater Splitting, *Inorg. Chem.* 60 (2021) 17371-17378.
- [22] L. Yu, Q. Zhu, S.W. Song, B. McElhenny, D.Z. Wang, C.Z. Wu, Z.J. Qin, J.M. Bao, Y. Yu, S. Chen, Z.F. Ren, Non-noble metal-nitride based electrocatalysts for high-performance alkaline seawater electrolysis, *Nat. Commun.* 10 (2019) 5106.

- [23] S. Anantharaj, S. R. Ede, K. Sakthikumar, K. Karthick, S. Mishra, S. Kundu, Recent Trends and Perspectives in Electrochemical Water Splitting with an Emphasis on Sulfide, Selenide, and Phosphide Catalysts of Fe, Co, and Ni: A Review, *ACS Catal.* 6 (2016) 8069-8097.
- [24] A. Sivanantham, S. Shanmugam, Nickel selenide supported on nickel foam as an efficient and durable non-precious electrocatalyst for the alkaline water electrolysis, *Appl. Catal. B: Environ.* 203 (2017) 485-493.
- [25] W.L. Ye, Y.N. Zhang, J.C. Fan, P.H. Shi, Y.L. Min, Q.J. Xu, Rod-like nickel doped  $\text{Co}_3\text{Se}_4$ /reduced graphene oxide hybrids as efficient electrocatalysts for oxygen evolution reactions, *Nanoscale*, 13 (2021) 3698-3708.
- [26] E. Aslan, A. Sarilmaz, G. Yanalak, C.S. Chang, I. Cinar, F. Ozel, I.H. Patir, Facile preparation of amorphous  $\text{NiWSe}_x$  and  $\text{CoWSe}_x$  nanoparticles for the electrocatalytic hydrogen evolution reaction in alkaline condition, *J. Electroanal. Chem.* 856 (2020) 113674.
- [27] J.L. Yang, H.C. Xuan, J.T. Yang, L.X. Meng, J. Wang, X.H. Liang, Y.P. Li, P.D. Han, Metal-organic framework-derived  $\text{FeS}_2/\text{CoNiSe}_2$  heterostructure nanosheets for highly-efficient oxygen evolution reaction, *Appl. Surf. Sci.* 578 (2022) 152016.
- [28] Y.R. Zheng, P. Wu, M.R. Gao, X.L. Zhang, F.Y. Gao, H.X. Ju, R. Wu, Q. Gao, R. You, W.X. Huang, S.J. Liu, S.W. Hu, J.F. Zhu, Z.Y. Li, S.H. Yu, Doping-induced structural phase transition in cobalt diselenide enables enhanced hydrogen evolution catalysis, *Nat. Commun.* 9 (2018) 2533.
- [29] Q.F. Gong, L.Cheng, C.H. Liu, M. Zhang, Q.L. Feng, H.L. Ye, M. Zeng, L.M. Xie, Z. Liu, Y.G. Li, Ultrathin  $\text{MoS}_{2(1-x)}\text{Se}_{2x}$  Alloy Nanoflakes For Electrocatalytic Hydrogen Evolution Reaction, *ACS Catal.* 5 (2015) 2213-2219.
- [30] E. Aslan, A. Sarilmaz, G. Yanalak, S.S. Ozel, F. Ozel, I.H. Patir, Transition metale-

- incorporated tungsten-based ternary refractory metal selenides ( $MWSe_x$ ;  $M = Fe, Co, Ni, \text{ and } Mn$ ) as hydrogen evolution catalysts at soft interfaces, *Mater. Today Energy* 18 (2020) 100510.
- [31] W.X. Li, B. Yu, Y. Hu, X.Q. Wang, D.X. Yang, Y.F. Chen, Core-Shell Structure of  $NiSe_2$  Nanoparticles@Nitrogen-Doped Graphene for Hydrogen Evolution Reaction in Both Acidic and Alkaline Media, *ACS Sustainable Chem. Eng.* 7 (2019) 4351-4359.
- [32] J. Yu, Q.Q. Li, C.Y. Xu, N. Chen, Y. Li, H.G. Liu, L. Zhen, V.P. Dravida, J.S. Wu,  $NiSe_2$  pyramids deposited on N-doped graphene encapsulated Ni foam for high-performance water oxidation, *J. Mater. Chem. A* 5 (2017), 3981.
- [33] J.H. Zhou, Z.G. Wang, D.X. Yang, Fei Qi, X. Hao, W.L. Zhang, Y.F. Chen,  $NiSe_2$ -anchored N, S-doped graphene/Ni foam as a free-standing bifunctional electrocatalyst for efficient water splitting, *Nanoscale* 12 (2020) 9866.
- [34] J. Deng, P.J. Ren, D.H. Deng, L. Yu, F. Yang, X.H. Bao, Highly active and durable non-precious-metal catalysts encapsulated in carbon nanotubes for hydrogen evolution reaction, *Energy Environ. Sci.* 7 (2014) 1919.
- [35] G.T. Zan, T. Wu, F. Zhu, P.F. He, Y.P. Cheng, S.S. Chai, Y. Wang, X.F. Huang, W.X. Zhang, Y. Wan, X.J. Peng, Q.S. Wu, A Biomimetic Conductive Super-foldable Material. *Matter*, 4(2021) 3232-3247.
- [36] G.T. Zan, T. Wu, W.Y. Dong, J.C. Zhou, T. Tu, R.X. Xu, Y. Chen, Y. Wang, Q.S. Wu, Two-Level Biomimetic Designs Enable Intelligent Stress Dispersion for Super-Foldable C/NiS Nanofiber Free-Standing Electrode, *Adv. Fiber Mater.* DOI: 10.1007/s42765-022-00162-7.
- [37] M. Kuang, Q.H. Wang, P. Han, G.F. Zheng, Cu, Co-Embedded N-Enriched Mesoporous Carbon for Efficient Oxygen Reduction and Hydrogen Evolution Reactions, *Adv. Energy Mater.* 7 (2017) 1700193.

- [38] F.L. Yang, Y.T. Chen, G.Z. Cheng, S.L. Chen, W. Luo, Ultrathin Nitrogen-Doped Carbon Coated with CoP for Efficient Hydrogen Evolution, *ACS Catal.* 7 (2017) 3824-3831.
- [39] J. Yu, W.J. Li, H.S. Zhang, F. Zhou, R.M. Li, C.Y. Xu, L.M. Zhou, H. Zhong, J. Wang, Metallic FePSe<sub>3</sub> nanoparticles anchored on N-doped carbon framework for All-pH hydrogen evolution reaction, *Nano Energy* 57 (2019) 222-229.
- [40] W.X. Yan, S.P. Chen, M. Wen, Q.S. Wu, S.H. Yu, Multicore closely packed ultrathin-MnO<sub>2</sub>@N-doped carbon-gear yolk-shell micro-nanostructures as highly efficient sulfur hosts for Li-S batteries, *J. Mater. Chem. A* 9 (2021) 2276.
- [41] Y.K. Tian, Y.X. Zhang, A.J. Huang, M. Wen, Q.S. Wu, L. Zhao, M.K. Wang, Y. Shen, Z.G. Wang, Y.Q. Fu, Nanostructured Ni<sub>2</sub>SeS on Porous-Carbon Skeletons as Highly Efficient Electrocatalyst for Hydrogen Evolution in Acidic Medium, *Inorg. Chem.* 59 (2020) 6018-6025.
- [42] Y.Y. Ma, C.X. Wu, X.J. Feng, H.Q. Tan, L.K. Yan, Y. Liu, Z.H. Kang, E.B. Wang, Y.G. Li, Highly efficient hydrogen evolution from seawater by a low-cost and stable CoMoP@C electrocatalyst superior to Pt/C, *Energy Environ. Sci.* 10 (2017) 788.
- [43] M. S. Vidhya, G. Ravi, R. Yuvakkumar, M. Thambidurai, C. Dang, M. Pannipara, A. G. Al-Sehemi, D. Velauthapillai, Energy storage performance of CoNiSe<sub>2</sub> nanostructures, *Mater. Lett.* 279 (2020) 128485.
- [44] B. J. Rani, G. Ravi, R. Yuvakkumar, B. Saravanakumar, M. Thambidurai, C. Dang, D. Velauthapillai, CoNiSe<sub>2</sub> Nanostructures for Clean Energy Production, *ACS Omega* 2020, 5, 14702-14710.
- [45] J.Y. Lee, N.Y. Kim, D.Y. Shin, H.-Y. Park, S.-S. Lee, S.J. Kwon, D.-H. Lim, K.W. Bong, J.G. Son, J.Y. Kim, Nitrogen-doped graphene-wrapped iron nanofragments for high-performance oxygen reduction electrocatalysts, *J. Nanopart. Res.*, 19 (2017) 98.

- [46] Z.J Guo, X.Y Feng, X.X Li, X.M Zhang, X. Peng, H. Song, J.J Fu, K. Ding, X. Huang, B. Gao, Nitrogen Doped Carbon Nanosheets Encapsulated in situ Generated Sulfur Enable High Capacity and Superior Rate Cathode for Li-S Batteries, *Front. Chem.*, 6 (2018) 429.
- [47] Y. Pan, K.A. Sun, S.J. Liu, X. Cao, K.L. Wu, W.C. Cheong, Z. Chen, Y. Wang, Y. Li, Y.Q. Liu, D.S. Wang, Q. Peng, C. Chen, Y.D. Li, Core-Shell ZIF-8@ZIF-67-Derived CoP Nanoparticle-Embedded N-Doped Carbon Nanotube Hollow Polyhedron for Efficient Overall Water Splitting, *J. Am. Chem. Soc.* 140 (2018) 2610-2618.
- [48] Y. Xu, Y.P. Mo, J. Tian, P. Wang, H.G. Yu, J.G. Yu, The synergistic effect of graphitic N and pyrrolic N for the enhanced photocatalytic performance of nitrogen-doped graphene/TiO<sub>2</sub> nanocomposites, *Appl. Catal. B: Environ.* 181 (2016) 810-817.
- [49] A. Sivanantham, P. Ganesan, S. Shanmugam, Hierarchical NiCo<sub>2</sub>S<sub>4</sub> Nanowire Arrays Supported on Ni Foam: An Efficient and Durable Bifunctional Electrocatalyst for Oxygen and Hydrogen Evolution Reactions, *Adv. Funct. Mater.* 26 (2016) 4661-4672.
- [50] B. Yu, X.Q. Wang, F. Qi, B.J. Zheng, J.R. He, J. Lin, W.L. Zhang, Y.R. Li, Y.F. Chen, Self-Assembled Coral-like Hierarchical Architecture Constructed by NiSe<sub>2</sub> Nanocrystals with Comparable Hydrogen-Evolution Performance of Precious Platinum Catalyst, *ACS Appl. Mater. Interfaces* 9 (2017) 7154-7159.
- [51] Y.Q. Yang, W.B. Zhang, Y.L. Xiao, Z.P. Shi, X.M. Cao, Y. Tang, Q.S. Gao, CoNiSe<sub>2</sub> heteronanorods decorated with layered-double-hydroxides for efficient hydrogen evolution, *Appl. Catal. B*, 242 (2019) 132-139.
- [52] Y. Hattori, T. Konishi, K. Kaneko, XAFS and XPS studies on the enhancement of methane adsorption by NiO dispersed ACF with the relevance to structural change of NiO, *Chem. Phys. Lett.* 355 (2002) 37-42.

- [53] C.L. Jiao, X.J. Bo, M. Zhou, Electrocatalytic water splitting at nitrogen-doped carbon layers-encapsulated nickel cobalt selenide, *J. Energy Chem.* 34 (2019) 161-170.
- [54] D.S. Kong, H.T. Wang, Z.Y. Lu, Y. Cui, CoSe<sub>2</sub> Nanoparticles Grown on Carbon Fiber Paper: An Efficient and Stable Electrocatalyst for Hydrogen Evolution Reaction, *J. Am. Chem. Soc.* 136 (2014) 4897-4900.
- [55] F.F. Zhang, Y. Pei, Y.C. Ge, H. Chu, S. Craig, P. Dong, J. Cao, P.M. Ajayan, M.X. Ye, J.F. Shen, Controlled Synthesis of Eutectic NiSe/Ni<sub>3</sub>Se<sub>2</sub> Self-Supported on Ni Foam: An Excellent Bifunctional Electrocatalyst for Overall Water Splitting, *Adv. Mater. Interfaces* 5 (2018) 1701507.
- [56] T. Shinagawa, A.T. Garcia-Esparza, K. Takane, Insight on Tafel slopes from a microkinetic analysis of aqueous electrocatalysis for energy Conversion, *Sci. Rep.* 5 (2015) 13801.
- [57] B.E. Conway, B.V. Tilak, Interfacial processes involving electrocatalytic evolution and oxidation of H<sub>2</sub>, and the role of chemisorbed H, *Electrochim. Acta* 47 (2002) 3571-3594.
- [58] X.G. Wang, Y.V. Kolen'ko, X.Q. Bao, K. Kovnir, L.F. Liu, One-Step Synthesis of Self-Supported Nickel Phosphide Nanosheet Array Cathodes for Efficient Electrocatalytic Hydrogen Generation, *Angew. Chem. Int. Ed.* 54 (2015) 8188-8192.
- [59] B.W. Lu, J.B. Zang, W. Li, J.L. Li, Q. Zou, Y.K. Zhou, Y.H. Wang, Co-doped Ni<sub>x</sub>P<sub>y</sub> loading on Co<sub>3</sub>O<sub>4</sub> embedded in Ni foam as a hierarchically porous self-supported electrode for overall water splitting, *Chem. Eng. J.* 422 (2021) 130062.
- [60] K. Seth, A.J. Darling, C.F. Holder, Y.H. Xiong, J.R. Shallenberger, R.E. Schaak, In Situ Evolution of Ru<sub>4</sub>Al<sub>13</sub> Crystals into a Highly Active Catalyst for the Hydrogen Evolution Reaction. *Chem. Mater.* 33(2021) 7124-7131.
- [61] B.H. He, L. Chen, M.J. Jing, M.J. Zhou, Z.H. Hou, X.B. Chen, 3D MoS<sub>2</sub>-rGO@Mo

nanohybrids for enhanced hydrogen evolution: The importance of the synergy on the Volmer reaction, *Electrochim. Acta.* 283 (2018) 357-365.

[62]J. Deng, P.J. Ren, D.H. Deng, X.H. Bao, Enhanced Electron Penetration through an Ultrathin Graphene Layer for Highly Efficient Catalysis of the Hydrogen Evolution Reaction, *Angew. Chem. Int. Ed.* 54 (2015) 2100-2104.

[63]L. Liang, H. Cheng, F.C. Lei, J. Han, S. Gao, C.M. Wang, Y.F. Sun, S. Qamar, S.Q. Wei, Y. Xie, Metallic Single-Unit-Cell Orthorhombic Cobalt Diselenide Atomic Layers: Robust Water-Electrolysis Catalysts, *Angew. Chem. Int. Ed.* 54 (2015) 12004-12008.